



Published in final edited form as:

*Ann Rheum Dis.* 2023 March ; 82(3): 403–415. doi:10.1136/ard-2022-223227.

## A senescent cell population with ZEB1 transcription factor as its main regulator promotes osteoarthritis in cartilage and meniscus

Hannah Swahn<sup>1</sup>, Kun Li<sup>1</sup>, Tomas Duffy<sup>1</sup>, Merissa Olmer<sup>1</sup>, Darryl D. D’Lima<sup>1,2</sup>, Tony S. Mondala<sup>3</sup>, Padmaja Natarajan<sup>3</sup>, Steven R. Head<sup>3</sup>, Martin K. Lotz<sup>1,\*</sup>

<sup>1</sup>Department of Molecular Medicine, Scripps Research, La Jolla, CA, 92037

<sup>2</sup>Shiley Center for Orthopaedic Research and Education at Scripps Clinic, Scripps Health, La Jolla, CA

<sup>3</sup>Center for Computational Biology & Bioinformatics and Genomics Core, Scripps Research, La Jolla, CA, 92037

### Abstract

**Objectives:** Single cell level analysis of articular cartilage and meniscus tissues from human healthy and osteoarthritis (OA) knees.

**Methods:** scRNA-seq analyses were performed on articular cartilage and meniscus tissues from healthy (n=6, n=7) and OA (n=6, n=6) knees. Expression of genes of interest was validated using IHC and RNA-seq and function was analyzed by gene overexpression and deletion.

**Results:** scRNA-seq analyses of human knee articular cartilage (70,972 cells) and meniscus (78,017 cells) identified a pathogenic subset that is shared between both tissues. This cell population is expanded in OA and has strong OA and senescence gene signatures. Further, this subset has critical roles in extracellular matrix (ECM) and tenascin signaling and is the dominant sender of signals to all other cartilage and meniscus clusters and a receiver of TGF $\beta$  signaling. Fibroblast activating protein (FAP) is also a dysregulated gene in this cluster and promotes ECM degradation. Regulons that are controlled by transcription factor ZEB1 are shared between the pathogenic subset in articular cartilage and meniscus. In meniscus and cartilage cells, FAP and ZEB1 promote expression of genes that contribute to OA pathogenesis, including senescence.

\*Correspondence to: Martin K Lotz, MD , Scripps Research, 10550 North Torrey Pines R, La Jolla, CA 92037, USA. mlotz@scripps.edu.

**Contributors:** M.K.L., T.D. and D.D.L. designed the study. H.S., T.D., M.O., T.S.M. and K.L. performed the experiments. H.S., and P.N. analyzed the data. S.R.H. and T.S.M. provided methodology. M.K.L. supervised the project. H.S. and M.K.L. drafted the paper, which was approved by all coauthors.

#### MATERIALS AND METHODS

Detailed materials and methods are available in the supplementary materials and methods.

**Competing interests:** The authors declare that they have no competing interests.

Ethics statements

**Patient consent for publication:** Obtained.

**Ethics approval:** All human tissues were obtained with approval by the Scripps Human Subjects Committee.

**Conclusions:** These single-cell studies identified a senescent pathogenic cell cluster that is present in cartilage and meniscus and has FAP and ZEB1 as main regulators which are novel and promising therapeutic targets for OA-associated pathways in both tissues.

### Keywords

Osteoarthritis; scRNA-seq; Chondrocytes; Meniscus; Senescence

---

## INTRODUCTION

Osteoarthritis (OA) affects all tissues in the knee joint<sup>1</sup> but therapeutic targets have often been selected for their role in cartilage damage and inflammation<sup>2</sup> and largely omitted consideration of mechanisms that are mediating meniscus damage and more importantly there have been insufficient efforts to determine whether pathogenic processes are shared between tissues. Mechanisms and molecules that are involved in such shared processes would conceptually represent more promising therapeutic targets.

Excessive mechanical stress, either chronically or caused by joint trauma is a major risk factor for OA and causes damage to menisci and cartilage<sup>3</sup>, the major tissues in the joint that absorb mechanical load.<sup>4</sup> Damage to one of these tissues leads to progressive changes in both.<sup>5</sup>

Global gene expression profiling has enabled discovery of new OA disease mechanisms. Bulk RNA sequencing analyses of human and rodent OA knees have revealed dysregulation in extracellular matrix, circadian rhythm pathways and mechanotransduction.<sup>6-9</sup> The limitation of bulk transcriptomic analysis is that it averages changes in global gene expression across tissues that are often highly heterogeneous in cell-type composition. Although useful for a broad view of disease impact, disease-related changes restricted to certain cell populations are often masked by these analyses. Single-cell RNA sequencing (scRNA-seq) technologies overcome these limitations.<sup>10</sup> Several scRNA-seq analyses have been performed in OA knees but have been largely restricted to the analysis of a single joint tissue of articular cartilage<sup>11-15</sup>, or meniscus<sup>16</sup> with the exception of one study that analyzed cartilage and synovium<sup>17</sup>. Here, we performed scRNA-seq analyses of healthy and OA-affected human knee cartilage and menisci to interrogate separate and shared mechanisms in cellular homeostasis and OA pathogenesis.

## RESULTS

### The cellular landscape in healthy articular cartilage

We performed scRNA-seq of healthy cartilage from 6 donors and analyzed 39,278 scRNA-seq profiles resulting in 10 clusters (Figure 1A). Each donor similarly contributed to each cluster (Figure 1B). We identified previously described cell populations<sup>11-15 17</sup> including regulatory (RegC), effector (EC), pre-fibrocartilage (preFC), fibrocartilage (FC), pre-hypertrophic (preHTC), hypertrophic (HTC), homeostatic (HomC) and reparative (RepC) chondrocytes (Figure 1C; Supplementary Table 1). We observed two populations of CHI3L1<sup>+</sup>, CHI3L2<sup>+</sup> RegCs. RegC-2 was distinguishable by its expression of

metallothionein genes. The biological processes associated with both were related to stress response; however, RegC-1 was primarily involved in inflammatory response, and RegC-2 was key in metal ion homeostasis. We also observed two populations of FCs. Both expressed *IGFBP5* and *S100A4*; however, FC-1 highly expressed *COL1A1*, *COL1A2* and *MSMP*. Similar to preFCs, FC-2 highly expressed *PRG4* and *SEMA3A*.

CellChat<sup>18</sup> interrogates cell-cell interactions for signals sent and signals received between cells (Supplemental Materials). preHTCs and preFCs were the strongest senders of signals, and preFCs, FCs and HomCs were the strongest receivers (Figure 1D). Twenty-four signaling pathways were enriched across all clusters, including collagen, FN1, THBS, tenascin, laminin, and TGF $\beta$  (Figure 1E), which are important in extracellular matrix (ECM) homeostasis. To understand the gene regulatory networks (GRN) that differentiate the clusters, we performed pySCENIC analysis<sup>19</sup> which identified 332 enriched regulons (Figures 1F–J; Supplementary Table 2). RepCs had the highest regulatory activity of all clusters (Figure 1F). Across other clusters, regulons were highly specific. For example, HTCs represent the terminal stage of chondrocyte differentiation, while FCs are the most fibroblastic. FC-1 and HTCs only had 2 overlapping active regulons (AUC > 1), while FC-2 and HTCs had no overlap (Figures 1G–J).

### The cellular landscape in healthy meniscus

We also performed scRNA-seq of meniscus from the same six cartilage donors and one additional healthy donor. A total of 45,426 scRNA-seq profiles were included in the analyses, resulting in 17 clusters (Figure 2A). Each donor similarly contributed to every cluster (Figure 2B). We identified previously described cell populations<sup>11–17</sup> including RegC, EC, preFC, FC, preHTC, HomC, RepC, proliferative chondrocytes (ProC), fibrocartilage progenitors (FCP), immune cells and endothelial cells (Figure 2C; Supplementary Table 3).

CellChat analysis<sup>18</sup> showed that preFCs, ProCs and FCs were the strongest senders of signals, while endothelial cells, FCs and preHTCs were the strongest receivers (Figure 2D). Fifty-eight signaling pathways were enriched across all meniscus clusters, including collagen and FN1 (Figure 2E). Unlike articular cartilage, immune signaling pathways (CXCL, TNF and CD45) were also enriched. pySCENIC analysis<sup>19</sup> identified 366 enriched regulons (Figure 2F; Supplementary Table 4). Regulons were cluster-specific, with immune cells having the highest regulatory activity.

### scRNA-seq of articular cartilage identifies an expanded pathogenic subset in OA with a senescence gene signature

We performed scRNA-seq of articular cartilage from 6 OA donors and compared data with the 6 healthy donors described above. Principal component analysis (PCA) revealed overlap between all donors and conditions (Supplementary Figures 1A, B). After quality control, we retained 70,972 cells for downstream analyses with an average of 13,024 counts/cell and 2,867 features/cell. We identified 13 clusters (Figure 3A). In addition to the populations in healthy cartilage, we identified a small population of ProCs, with biological processes related to response to unfolded protein, regulation of transcription, metabolomics,

and cell proliferation. Additionally, we identified a population of chondrocytes with high expression of metallothioneins (MTC). Unlike RegC-2, MTC lacked expression of *CHI3L1* and *CHI3L2*. The biological processes included metal ion homeostasis, response to hypoxia and regulation of apoptosis. All 13 clusters were present in both normal and OA cells (Figure 3B; Supplementary Figures 1C, G) with ~55% of the cells originating from healthy donors, and ~45% of the cells originating from OA donors (Supplementary Figures 1D, E). The largest clusters were MTCs and ECs (Supplementary Figure 1F). MTCs were depleted in OA. In contrast, one subpopulation (black boxes) was expanded in OA (Figure 3B; Supplementary Figure 1F). Differential abundance of cell neighborhoods within this population in OA compared to healthy was statistically significant using Milo analysis<sup>20</sup> (blue boxes) (Figures 3C–D). This population was deemed a pathogenic subset as it had the strongest enrichment among all subsets of 134 OA-associated genes which were compiled using a list of DEGs from a bulk RNA-sequencing analysis of normal and OA human cartilage<sup>6</sup> (Figure 3E; Supplementary Table 5). One of these highly expressed genes was periostin (*POSTN*), which was largely absent in other clusters (Figure 3F). There were 606 significant markers for this pathogenic cluster (Supplementary Figure 2; Supplementary Table 6).

We investigated the senescence profile of this pathogenic subpopulation, including expression of core, associated and senescence-associated secretory phenotype (SASP) genes<sup>21 22</sup> across all clusters in both normal and OA and visualized expression in a bubble plot (Figure 3G; Supplementary Table 5). We observed upregulation of many of these in OA compared to normal, suggesting a strong senescence signature, notably enhancement in expression of *CDKN2A* (p16) and depletion of *CDKN1A* (p21) in the pathogenic cluster in OA (black boxes).

Finally, to understand the biological processes dysregulated in this pathogenic cluster, we performed gene ontology (GO) analysis (Supplementary Table 7). 3,454 genes were considered DE at an adjusted p value < 0.05 (751 downregulated, 2,703 upregulated). Biological pathways downregulated in OA were related to stimulus response, metabolomics, cell death and RNA (Figure 3H; Supplementary Table 7). In contrast, the upregulated processes were related to translation, mitochondrial function, and ECM properties (Figure 3I; Supplementary Table 7).

### **scRNA-seq of meniscus identifies a similar expanded pathogenic subset in OA with a senescence gene signature and dysregulated ECM genes**

We performed scRNA-seq of meniscus tissues from the same healthy and OA cartilage donors. PCA revealed overlap between all donors and conditions (Supplementary Figures 3A, B). After quality control, we retained 78,017 cells for downstream analyses with an average of 10,184 counts/cell and 2,588 features/cell. Our analysis identified 19 clusters (Figure 4A), including all populations in our healthy meniscus data sets. Additionally, we identified MTCs. All 19 clusters were present in both normal and OA cells (Figure 4B; Supplementary Figures 3C, G) with ~58% of the cells originating from healthy donors, and ~42% of the cells originating from OA donors (Supplementary Figures 3D, E). The largest cluster was RepCs (Supplementary Figure 4F). Several clusters were depleted in

OA including RepCs, MTCs, ProCs and HomCs. We observed a higher accumulation of immune cells in OA. The pathogenic subset was expanded in OA compared to normal (black boxes) (Figure 4B; Supplementary Figure 3F) and this was statistically significant using Milo analysis<sup>20</sup> (blue boxes) (Figures 4C, D).

The pathogenic subset had enrichment of 134 OA-associated genes (Figure 4E; Supplementary Table 5). This included *POSTN*, which was largely absent in other clusters (Figure 4F). There were 632 significant markers for this pathogenic cluster (Supplementary Figure 4; Supplementary Table 8). 270 of these were shared with the pathogenic cluster in cartilage (Supplementary Figure 5A), and were enriched for biological processes related to ECM, cell adhesion, oxidative phosphorylation, and wound response (Supplementary Figures 5B, C).

The senescence profile of this pathogenic population included upregulation in expression of many core-associated and SASP genes<sup>21 22</sup> (Supplementary Table 5) (Figure 4G). We also observed enhancement of *CDKN2A* and depletion of *CDKN1A* in the pathogenic cluster (black boxes).

GO analysis on 2,539 genes that were DE between normal and OA in the pathogenic cluster at an adjusted p value < 0.05 (781 downregulated, 1,758 upregulated; Supplementary Table 9) revealed that metabolomics, response to stress, cell death and RNA metabolomics were downregulated (Figure 4H; Supplementary Table 9). Upregulated processes were related to morphogenesis, actin dynamics, ECM properties and mitochondrial function (Figure 4I; Supplementary Table 9).

We investigated the ECM-related genes upregulated in the pathogenic subset and intersected the lists of genes associated with the GO term ‘extracellular matrix properties’ (GO:0030198) in articular cartilage and meniscus (Supplementary Table 10). This revealed 63 ECM genes dysregulated in the pathogenic cluster. These genes included many core matrix genes such as collagens, glycoproteins and proteoglycans and cell-matrix interaction genes including integrins, as well as genes that play regulatory roles in ECM homeostasis.

### **FAP promotes OA pathogenesis genes, including *MMP9* and *IL6***

FAP was chosen for further studies based on criteria including adjusted p value, log<sub>2</sub>FC and percentage difference in cells expressing this gene in OA compared to normal. FAP has been linked to poor prognosis in rheumatoid arthritis and has been shown to be upregulated in rheumatoid myofibroblast-like synoviocytes.<sup>23 24</sup> FAP expression was upregulated in OA cartilage in all clusters (Figure 5A, upper) and specifically in the pathogenic population (Figure 5A, lower). This enhancement in FAP was validated at the protein level using immunohistochemistry (IHC) (Figures 5B, C). FAP expression was similarly upregulated in OA meniscus in all clusters (Figure 5D, upper) and specifically in the pathogenic population (Figure 5D, lower). This upregulation was confirmed by IHC (Figures 5E, F).

To characterize the function of FAP in chondrocytes, TC28a2 cells were transfected with FAP and global transcriptome was analyzed by bulk digital RNA with perturbation of

genes and sequencing (DRUG-seq) analysis<sup>25</sup>. 78 genes were considered differentially expressed (adjusted p value < 0.05). Upregulation of FAP mRNA was confirmed (Figure 5G). Expression of all DEGs was visualized in a volcano plot (Figure 5H). Biological processes downregulated by FAP were related to response to hypoxia (Figure 5I), while those upregulated were related to degradation of extracellular matrix and cell adhesion (Figure 5J).

Since the DRUG-seq data suggested FAP upregulates genes involved in degradation of ECM, we next independently validated these data in TC28a2 cells, primary chondrocytes and meniscus cells. In TC28a2, activation of FAP significantly enhanced *MMP9* expression (Figure 5K). Similarly, depletion of FAP in TC28a2 cells using a shRNA suppressed *MMP9* (Figure 5L). Transfection of FAP in normal chondrocytes (Figure 5M), normal meniscus (Figure 5O), OA chondrocytes (Figure 5N) and OA meniscus (Figure 5P) significantly upregulated *MMP9* which cleaves types I and III collagens<sup>26</sup>. We also observed enhancement in *IL6* expression in normal chondrocytes (Figure 5M), normal meniscus (Figure 5O), OA chondrocytes (Figure 5N) and OA meniscus (Figure 5P). IL-6 increases *MMP9* expression.<sup>27</sup>

### The pathogenic subset plays critical roles in collagen, TGF $\beta$ and tenascin signaling

To investigate how this subset communicates with other cell populations, we performed CellChat analysis<sup>18</sup> (Figures 6A, I). Across all enriched signals, the pathogenic population was among the strongest receivers and senders of signals in both tissue types (Figures 6B, J), indicating that it has critical roles in overall cell communication. We next identified which signals were contributing to the incoming or outgoing signaling networks and visualized these data on a heat-map (Figures 6C, K). The top enriched signaling pathway in both tissue types was collagen, which was expected as collagens are critical components of the matrisome, and it is well established that OA is characterized by dysregulation of ECM properties. Looking specifically at the pathogenic subset, this analysis revealed critical roles in several other networks including TGF $\beta$  and tenascin signaling.

We next sought to determine the relative importance of this pathogenic subset in the four CellChat-defined centrality measures (Figure 6D) of the collagen, TGF $\beta$  and tenascin signaling networks. This analysis revealed that the pathogenic population was a critical sender and receiver of collagen signaling in both tissues (Figures 6E, L). In addition to being a critical receiver of collagen signaling, this pathogenic subset was, effectively, the only receiver of TGF $\beta$  signaling (Figures 6F, M). This subset was also a critical sender of many signals, including tenascin. As visualized in circle plots (Figures 6G, N; upper panels) and heat-maps (Figures 6G, N; lower panels), the pathogenic subset appeared to be a dominant sender of tenascin signaling, specifically tenascin C (TNC) (Figures 6H, O). The top receivers of the tenascin signal originating from the pathogenic population were homeostatic, metallothionein, reparative, and pre-hypertrophic chondrocytes (Figures 6H, O). Additionally, the pathogenic population was a receiver of its own signal, suggesting a potential positive feedback loop.

## The pathogenic subset has regulatory programs shared in both tissue types including members of the CREB family and ZEB1

Gene regulatory networks (GRN) in the pathogenic subset were analyzed by pySCENIC<sup>19</sup>. Of the 342 significant regulons enriched across all articular cartilage clusters (Supplementary Table 11), 102 were enriched in the pathogenic cluster (AUC score > 0.5) (Figure 7A). Many of the enriched regulons include driving TFs that are involved in OA including CREB family members (CREB3, CREB3L1 and CREB3L2). Another example of an important enriched TF is ZEB1, a regulator of senescence.<sup>28 29</sup> In meniscus, 350 regulons were enriched across all clusters (Supplementary Table 12), with 72 enriched in the pathogenic cluster (Figure 7B). 32 of these 72 were shared with the pathogenic cluster in articular cartilage (44%) (Figure 7C). The large proportion of shared regulons identifies TFs as promising therapeutic targets for OA-associated pathways in both tissues.

## ZEB1 is a key regulator of cell senescence through promotion of mitochondrial dysregulation and induction of CDKN2A expression

ZEB1 expression was upregulated in OA articular cartilage compared to healthy in all clusters (Figure 8A, left) and specifically in the pathogenic population (Figure 8A, right). This enhancement in ZEB1 was validated by IHC (Figures 8B, C). ZEB1 protein was significantly higher in an OA-affected area (OA) compared to a normal-appearing area (OA-N) from the same donor. ZEB1 expression was similarly upregulated in OA meniscus compared to healthy in all clusters (Figure 8D, left) and in the pathogenic population (Figure 8D, right). This was associated with upregulation of ZEB1 protein (Supplementary Figures 6A, B).

To examine the role of ZEB1 in chondrocytes, TC28a2 cells were transfected with ZEB1 plasmid. DRUG-seq analysis<sup>25</sup> revealed 156 differentially expressed genes (adjusted p value < 0.05; Supplementary Table 13). ZEB1 was the top DEG (Figure 8E). All DEGs were visualized on a volcano plot (Figure 8F). GO analysis revealed the biological processes downregulated by ZEB1 included endoderm differentiation, apoptosis, and cell migration (Figure 8G). In contrast, the upregulated processes were translation and mitochondrial function (Figure 8H).

We investigated the specific role of ZEB1 in mitochondrial function. The oxidative phosphorylation (OXPHOS)<sup>31</sup> system consists of five multiprotein complexes (Supplementary Figure 7A). In TC28a2 cells, ZEB1 overexpression preferentially upregulated members of complexes I (NADH: ubiquinone oxidoreductase) and III (cytochrome bc1 complex), the major sources of reactive oxygen species (ROS).<sup>32-34</sup> ZEB1 significantly upregulated 11/37 nuclear-encoded genes of mitochondrial complex I (Supplementary Figure 8A), 4/9 nuclear-encoded complex III members (Supplementary Figure 8C) and also a few members of complexes II, IV and V (Supplementary Figures 8B, D, E).

In the pathogenic cluster in both articular cartilage and meniscus, the mean expression of all nuclear-encoded complex I and III genes was significantly higher in OA compared to normal (Supplementary Figures 7B, D). These data suggest that the enhanced expression of these

complex members in the pathogenic cluster is, in part, due to increased ZEB1 expression. As excess ROS and oxidative stress are functional consequences of enhanced metabolism, ZEB1 potentially promotes mitochondrial dysfunction through ROS-producing complexes I and III.

In redox signaling (Supplementary Figures 9A–C), ZEB1 only altered *SOD1*. However, expression of antioxidants (particularly *SOD2*), oxidative stress response genes, and oxygen transporters were downregulated in the pathogenic cluster in OA compared to normal (Supplementary Figures 9D–I). Taken together, these data suggest that ZEB1 enhances ROS production but does not significantly affect protection against oxidative stress.

Since the DRUG-seq data suggested ZEB1 upregulates genes involved in mitochondrial function, and there is a significant senescence signature in the pathogenic population, we interrogated the role of ZEB1 in cell senescence. We overexpressed ZEB1 in TC28a2 cells, primary healthy chondrocytes and primary healthy meniscus cells. ZEB1 transfection of TC28a2 (Figure 8I) significantly enhanced expression of *CDKN2A*, *MMP2*, and *SERPINE1*. In parallel, ZEB1 was depleted using a shRNA (Figure 8J) and significant downregulation of *CDKN2A*, *RELA*, *IL6* and *SERPINE1* was observed. To further validate these data, ZEB1 expression was depleted using CRISPRi (Figure 8K) and this significantly reduced *CDKN2A*, *MMP9* and *IL6*. To validate these data in primary cells, we performed the overexpression assays in primary articular cartilage and in primary meniscus cells. In chondrocytes, ZEB1 significantly enhanced *CDKN2A*, *RELA*, *MMP2*, *MMP9*, *IL6* and *SERPINE1*, but expression of *CDKN1A* was unchanged (Figure 8L). In meniscus, ZEB1 significantly upregulated *MMP9*, *IL6* and *SERPINE1* (Figure 8M). Expression of *CDKN1A* was unchanged. Taken together, these data suggest that ZEB1 is a key regulator of cell senescence through promotion of mitochondrial dysfunction and induction of *CDKN2A* and SASP gene expression.

## DISCUSSION

This study used healthy human cartilage and meniscus from the same adult human donors to determine the normal cellular composition of the tissues and mechanisms of tissue homeostasis. In a parallel approach, matching cartilage and meniscus from the same OA joints were analyzed for disease mechanisms that are unique and shared between the tissues. In our analysis of OA samples, the first parameter we investigated was numerical changes in the cell clusters. In OA articular cartilage, the MTC subset was reduced in cell numbers whereas, the pathogenic subset was increased. In OA meniscus, multiple cell populations were significantly altered in OA. ProCs, HomCs, MTCs and RepCs were reduced, but immune cells and the pathogenic subset were enhanced in OA. MTCs were reduced in OA in both tissues. This population is marked by high expression of metallothionines, metal-binding proteins that act as buffers against toxic heavy metals and protect against oxidative stress.<sup>35 36</sup> As oxidative stress is a hallmark of OA disease progression<sup>37</sup>, loss of this protective subset likely contributes to disease pathogenesis. In addition to reduction of a protective population, we observed significant expansion of a pathogenic population in both tissue types. As this was the only shared expanded subset, we performed analyses to characterize the genes and biological properties in this population.

The pathogenic population had significant dysregulation in ECM properties – specifically, an upregulation of fibrotic collagens and matrix degrading enzymes. One of these genes was *FAP*, which encodes fibroblast activation protein alpha, a cell surface glycoprotein serine protease<sup>38 39</sup> involved in ECM degradation<sup>46–49</sup>. Activation of FAP in chondrocytes and meniscus cells increased MMP9, suggesting that ECM dysregulation observed in the pathogenic subset is, at least in part, mediated through FAP and MMP9.

CellChat analysis suggested that the pathogenic subset was effectively the only receiver of TGF $\beta$  signaling in both tissue types. As TGF $\beta$  is the central mediator of fibrosis, and is upregulated in many fibrotic diseases<sup>50</sup>, this suggests that the pathogenic subset is likely a fibrotic population. In addition to a fibrotic-like phenotype, CellChat analysis revealed that the pathogenic subset is involved in mechanotransduction through tenascin signaling, specifically through TNC, a critical component in the mechanosome.

The pathogenic population had a significant senescence signature in both tissue types. The regulons that were most active in the OA pathogenic cluster shared upregulation of ZEB1. This TF was predicted to bind to the promoters of the pathogenic genes in this cluster. Notably, it is a factor that has been implicated in senescence<sup>28 29</sup>, a key feature of the pathogenic cluster in both tissue types. We also investigated if ZEB1 could promote senescence by ZEB1 overexpression and depletion. ZEB1 enhanced expression of core senescence gene, *CDKN2A* (p16), but not *CDKN1A* (p21), suggesting that ZEB1 also plays a direct role in promoting senescence in a p16-dependent manner.

It is important to acknowledge the limitations of this study. First, the enzymatic digestion required to obtain single cells could cause bias towards certain chondrocyte subpopulations and alter gene expression.<sup>51 52</sup> The mean age of the healthy donors was much lower than of the OA donors and it is thus difficult to determine whether the observed changes are aging-related or OA-associated. However, the changes in ZEB1 and its influence on cell senescence appear to be due to OA. Despite these limitations, our integrative scRNA-seq analyses of articular cartilage and meniscus tissues have revealed a novel pathogenic, senescent subset that is expanded in OA. FAP and ZEB1 are main regulators which are novel and promising therapeutic targets for OA-associated pathways in both tissues.

## Supplementary Material

Refer to Web version on PubMed Central for supplementary material.

## Acknowledgements:

We thank Harry Celestin, Michelle Payad, Zaira Flores, Jessica Nitta and the team at Lifesharing, San Diego for human tissue procurement.

## Funding:

National Institutes of Health grant R01AG049617.

## Data availability statement:

All data relevant to the study are included in the article or uploaded as online supplemental information. The GEO accession numbers for all the datasets utilized in the present study will be made available upon acceptance of the manuscript and included in the final version.

## REFERENCES

1. Katz JN, Arant KR, Loeser RF. Diagnosis and Treatment of Hip and Knee Osteoarthritis: A Review. *JAMA* 2021;325(6):568–78. doi: 10.1001/jama.2020.22171 [published Online First: 2021/02/10] [PubMed: 33560326]
2. Latourte A, Kloppenburg M, Richette P. Emerging pharmaceutical therapies for osteoarthritis. *Nat Rev Rheumatol* 2020;16(12):673–88. doi: 10.1038/s41584-020-00518-6 [published Online First: 2020/10/31] [PubMed: 33122845]
3. Brophy RH, Huston LJ, Briskin I, et al. Articular Cartilage and Meniscus Predictors of Patient-Reported Outcomes 10 Years After Anterior Cruciate Ligament Reconstruction: A Multicenter Cohort Study. *Am J Sports Med* 2021;49(11):2878–88. doi: 10.1177/03635465211028247 [published Online First: 2021/07/30] [PubMed: 34324369]
4. Sukopp M, Schall F, Hacker SP, et al. Influence of Menisci on Tibiofemoral Contact Mechanics in Human Knees: A Systematic Review. *Front Bioeng Biotechnol* 2021;9:765596. doi: 10.3389/fbioe.2021.765596 [published Online First: 2021/12/21] [PubMed: 34926419]
5. Ozeki N, Koga H, Sekiya I. Degenerative Meniscus in Knee Osteoarthritis: From Pathology to Treatment. *Life (Basel)* 2022;12(4) doi: 10.3390/life12040603 [published Online First: 2022/04/24]
6. Fisch KM, Gamini R, Alvarez-Garcia O, et al. Identification of transcription factors responsible for dysregulated networks in human osteoarthritis cartilage by global gene expression analysis. *Osteoarthritis Cartilage* 2018;26(11):1531–38. doi: 10.1016/j.joca.2018.07.012 [published Online First: 2018/08/07] [PubMed: 30081074]
7. Loeser RF, Olex AL, McNulty MA, et al. Disease progression and phasic changes in gene expression in a mouse model of osteoarthritis. *PLoS One* 2013;8(1):e54633. doi: 10.1371/journal.pone.0054633 [published Online First: 2013/02/06] [PubMed: 23382930]
8. Salazar-Noratto GE, De Nijs N, Stevens HY, et al. Regional gene expression analysis of multiple tissues in an experimental animal model of post-traumatic osteoarthritis. *Osteoarthritis Cartilage* 2019;27(2):294–303. doi: 10.1016/j.joca.2018.10.007 [published Online First: 2018/11/19] [PubMed: 30448533]
9. Appleton CT, Pitelka V, Henry J, et al. Global analyses of gene expression in early experimental osteoarthritis. *Arthritis Rheum* 2007;56(6):1854–68. doi: 10.1002/art.22711 [published Online First: 2007/05/29] [PubMed: 17530714]
10. Rai MF, Wu CL, Capellini TD, et al. Single Cell Omics for Musculoskeletal Research. *Curr Osteoporos Rep* 2021;19(2):131–40. doi: 10.1007/s11914-021-00662-2 [published Online First: 2021/02/10] [PubMed: 33559841]
11. Sunkara V, Heinz GA, Heinrich FF, et al. Combining segmental bulk- and single-cell RNA-sequencing to define the chondrocyte gene expression signature in the murine knee joint. *Osteoarthritis Cartilage* 2021;29(6):905–14. doi: 10.1016/j.joca.2021.03.007 [published Online First: 2021/03/26] [PubMed: 33762205]
12. Liu W, Chen Y, Zeng G, et al. Single-Cell Profiles of Age-Related Osteoarthritis Uncover Underlying Heterogeneity Associated With Disease Progression. *Front Mol Biosci* 2021;8:748360. doi: 10.3389/fmolb.2021.748360 [published Online First: 2022/01/28] [PubMed: 35083277]
13. Sebastian A, McCool JL, Hum NR, et al. Single-Cell RNA-Seq Reveals Transcriptomic Heterogeneity and Post-Traumatic Osteoarthritis-Associated Early Molecular Changes in Mouse Articular Chondrocytes. *Cells* 2021;10(6) doi: 10.3390/cells10061462 [published Online First: 2021/07/03]
14. Ji Q, Zheng Y, Zhang G, et al. Single-cell RNA-seq analysis reveals the progression of human osteoarthritis. *Ann Rheum Dis* 2019;78(1):100–10. doi: 10.1136/annrheumdis-2017-212863 [published Online First: 2018/07/22] [PubMed: 30026257]

15. Wang X, Ning Y, Zhang P, et al. Comparison of the major cell populations among osteoarthritis, Kashin-Beck disease and healthy chondrocytes by single-cell RNA-seq analysis. *Cell Death Dis* 2021;12(6):551. doi: 10.1038/s41419-021-03832-3 [published Online First: 2021/05/29] [PubMed: 34045450]
16. Sun H, Wen X, Li H, et al. Single-cell RNA-seq analysis identifies meniscus progenitors and reveals the progression of meniscus degeneration. *Ann Rheum Dis* 2020;79(3):408–17. doi: 10.1136/annrheumdis-2019-215926 [published Online First: 2019/12/25] [PubMed: 31871141]
17. Chou CH, Jain V, Gibson J, et al. Synovial cell cross-talk with cartilage plays a major role in the pathogenesis of osteoarthritis. *Sci Rep* 2020;10(1):10868. doi: 10.1038/s41598-020-67730-y [published Online First: 2020/07/04] [PubMed: 32616761]
18. Jin S, Guerrero-Juarez CF, Zhang L, et al. Inference and analysis of cell-cell communication using CellChat. *Nat Commun* 2021;12(1):1088. doi: 10.1038/s41467-021-21246-9 [published Online First: 2021/02/19] [PubMed: 33597522]
19. Van de Sande B, Flerin C, Davie K, et al. A scalable SCENIC workflow for single-cell gene regulatory network analysis. *Nat Protoc* 2020;15(7):2247–76. doi: 10.1038/s41596-020-0336-2 [published Online First: 2020/06/21] [PubMed: 32561888]
20. Dann E, Henderson NC, Teichmann SA, et al. Differential abundance testing on single-cell data using k-nearest neighbor graphs. *Nat Biotechnol* 2022;40(2):245–53. doi: 10.1038/s41587-021-01033-z [published Online First: 2021/10/02] [PubMed: 34594043]
21. Hernandez-Segura A, de Jong TV, Melov S, et al. Unmasking Transcriptional Heterogeneity in Senescent Cells. *Curr Biol* 2017;27(17):2652–60 e4. doi: 10.1016/j.cub.2017.07.033 [published Online First: 2017/08/29] [PubMed: 28844647]
22. Hernandez-Segura A, Nehme J, Demaria M. Hallmarks of Cellular Senescence. *Trends Cell Biol* 2018;28(6):436–53. doi: 10.1016/j.tcb.2018.02.001 [published Online First: 2018/02/27] [PubMed: 29477613]
23. Bauer S, Jendro MC, Wadle A, et al. Fibroblast activation protein is expressed by rheumatoid myofibroblast-like synoviocytes. *Arthritis Res Ther* 2006;8(6):R171. doi: 10.1186/ar2080 [published Online First: 2006/11/16] [PubMed: 17105646]
24. Waldele S, Koers-Wunrau C, Beckmann D, et al. Deficiency of fibroblast activation protein alpha ameliorates cartilage destruction in inflammatory destructive arthritis. *Arthritis Res Ther* 2015;17:12. doi: 10.1186/s13075-015-0524-6 [published Online First: 2015/01/21] [PubMed: 25600705]
25. Ye C, Ho DJ, Neri M, et al. DRUG-seq for miniaturized high-throughput transcriptome profiling in drug discovery. *Nat Commun* 2018;9(1):4307. doi: 10.1038/s41467-018-06500-x [published Online First: 2018/10/20] [PubMed: 30333485]
26. Bigg HF, Rowan AD, Barker MD, et al. Activity of matrix metalloproteinase-9 against native collagen types I and III. *FEBS J* 2007;274(5):1246–55. doi: 10.1111/j.1742-4658.2007.05669.x [published Online First: 2007/02/15] [PubMed: 17298441]
27. Kossakowska AE, Edwards DR, Prusinkiewicz C, et al. Interleukin-6 regulation of matrix metalloproteinase (MMP-2 and MMP-9) and tissue inhibitor of metalloproteinase (TIMP-1) expression in malignant non-Hodgkin's lymphomas. *Blood* 1999;94(6):2080–9. [published Online First: 1999/09/09] [PubMed: 10477738]
28. Liu Y, El-Naggar S, Darling DS, et al. Zeb1 links epithelial-mesenchymal transition and cellular senescence. *Development* 2008;135(3):579–88. doi: 10.1242/dev.007047 [published Online First: 2008/01/15] [PubMed: 18192284]
29. de Barrios O, Gyroffy B, Fernandez-Acenero MJ, et al. ZEB1-induced tumorigenesis requires senescence inhibition via activation of DKK1/mutant p53/Mdm2/CtBP and repression of macroH2A1. *Gut* 2017;66(4):666–82. doi: 10.1136/gutjnl-2015-310838 [published Online First: 2016/12/15] [PubMed: 27965283]
30. Fernandez-Moreno M, Rego-Perez I, Blanco FJ. Is osteoarthritis a mitochondrial disease? What is the evidence. *Curr Opin Rheumatol* 2022;34(1):46–53. doi: 10.1097/BOR.0000000000000855 [published Online First: 2021/11/10] [PubMed: 34750310]

31. Fernandez-Vizarrá E, Tiranti V, Zeviani M. Assembly of the oxidative phosphorylation system in humans: what we have learned by studying its defects. *Biochim Biophys Acta* 2009;1793(1):200–11. doi: 10.1016/j.bbamcr.2008.05.028 [published Online First: 2008/07/16] [PubMed: 18620006]
32. Kowaltowski AJ, de Souza-Pinto NC, Castilho RF, et al. Mitochondria and reactive oxygen species. *Free Radic Biol Med* 2009;47(4):333–43. doi: 10.1016/j.freeradbiomed.2009.05.004 [published Online First: 2009/05/12] [PubMed: 19427899]
33. Murphy MP. How mitochondria produce reactive oxygen species. *Biochem J* 2009;417(1):1–13. doi: 10.1042/BJ20081386 [published Online First: 2008/12/09] [PubMed: 19061483]
34. Brand MD. The sites and topology of mitochondrial superoxide production. *Exp Gerontol* 2010;45(7–8):466–72. doi: 10.1016/j.exger.2010.01.003 [published Online First: 2010/01/13] [PubMed: 20064600]
35. Thirumoorthy N, Manisenthil Kumar KT, Shyam Sundar A, et al. Metallothionein: an overview. *World J Gastroenterol* 2007;13(7):993–6. doi: 10.3748/wjg.v13.i7.993 [published Online First: 2007/03/22] [PubMed: 17373731]
36. Ruttkay-Nedecký B, Nejdli L, Gumulec J, et al. The role of metallothionein in oxidative stress. *Int J Mol Sci* 2013;14(3):6044–66. doi: 10.3390/ijms14036044 [published Online First: 2013/03/19] [PubMed: 23502468]
37. Zahan OM, Serban O, Gherman C, et al. The evaluation of oxidative stress in osteoarthritis. *Med Pharm Rep* 2020;93(1):12–22. doi: 10.15386/mpr-1422 [published Online First: 2020/03/07] [PubMed: 32133442]
38. Rettig WJ, Chesa PG, Beresford HR, et al. Differential expression of cell surface antigens and glial fibrillary acidic protein in human astrocytoma subsets. *Cancer Res* 1986;46(12 Pt 1):6406–12. [published Online First: 1986/12/01] [PubMed: 2877731]
39. Pure E, Blomberg R. Pro-tumorigenic roles of fibroblast activation protein in cancer: back to the basics. *Oncogene* 2018;37(32):4343–57. doi: 10.1038/s41388-018-0275-3 [published Online First: 2018/05/04] [PubMed: 29720723]
40. Niedermeyer J, Garin-Chesa P, Kriz M, et al. Expression of the fibroblast activation protein during mouse embryo development. *Int J Dev Biol* 2001;45(2):445–7. [published Online First: 2001/05/02] [PubMed: 11330865]
41. Mathew S, Scanlan MJ, Mohan Raj BK, et al. The gene for fibroblast activation protein alpha (FAP), a putative cell surface-bound serine protease expressed in cancer stroma and wound healing, maps to chromosome band 2q23. *Genomics* 1995;25(1):335–7. doi: 10.1016/0888-7543(95)80157-h [published Online First: 1995/01/01] [PubMed: 7774951]
42. Levy MT, McCaughan GW, Abbott CA, et al. Fibroblast activation protein: a cell surface dipeptidyl peptidase and gelatinase expressed by stellate cells at the tissue remodeling interface in human cirrhosis. *Hepatology* 1999;29(6):1768–78. doi: 10.1002/hep.510290631 [published Online First: 1999/05/29] [PubMed: 10347120]
43. Acharya PS, Zukas A, Chandan V, et al. Fibroblast activation protein: a serine protease expressed at the remodeling interface in idiopathic pulmonary fibrosis. *Hum Pathol* 2006;37(3):352–60. doi: 10.1016/j.humpath.2005.11.020 [published Online First: 2006/04/15] [PubMed: 16613331]
44. Wang XM, Yao TW, Nadvi NA, et al. Fibroblast activation protein and chronic liver disease. *Front Biosci* 2008;13:3168–80. doi: 10.2741/2918 [published Online First: 2007/11/06] [PubMed: 17981786]
45. Jacob M, Chang L, Pure E. Fibroblast activation protein in remodeling tissues. *Curr Mol Med* 2012;12(10):1220–43. doi: 10.2174/156652412803833607 [published Online First: 2012/07/28] [PubMed: 22834826]
46. Aggarwal S, Brennen WN, Kole TP, et al. Fibroblast activation protein peptide substrates identified from human collagen I derived gelatin cleavage sites. *Biochemistry* 2008;47(3):1076–86. doi: 10.1021/bi701921b [published Online First: 2007/12/22] [PubMed: 18095711]
47. Christiansen VJ, Jackson KW, Lee KN, et al. Effect of fibroblast activation protein and alpha2-antiplasmin cleaving enzyme on collagen types I, III, and IV. *Arch Biochem Biophys* 2007;457(2):177–86. doi: 10.1016/j.abb.2006.11.006 [published Online First: 2006/12/19] [PubMed: 17174263]

48. Brokopp CE, Schoenauer R, Richards P, et al. Fibroblast activation protein is induced by inflammation and degrades type I collagen in thin-cap fibroatheromata. *Eur Heart J* 2011;32(21):2713–22. doi: 10.1093/eurheartj/ehq519 [published Online First: 2011/02/05] [PubMed: 21292680]
49. Fan MH, Zhu Q, Li HH, et al. Fibroblast Activation Protein (FAP) Accelerates Collagen Degradation and Clearance from Lungs in Mice. *J Biol Chem* 2016;291(15):8070–89. doi: 10.1074/jbc.M115.701433 [published Online First: 2015/12/15] [PubMed: 26663085]
50. Biernacka A, Dobaczewski M, Frangogiannis NG. TGF-beta signaling in fibrosis. *Growth Factors* 2011;29(5):196–202. doi: 10.3109/08977194.2011.595714 [published Online First: 2011/07/12] [PubMed: 21740331]
51. Jakob M, Demartean O, Schafer D, et al. Enzymatic digestion of adult human articular cartilage yields a small fraction of the total available cells. *Connect Tissue Res* 2003;44(3–4):173–80. doi: 10.1080/03008200390215836 [published Online First: 2003/09/25] [PubMed: 14504038]
52. Tsuyuguchi Y, Nakasa T, Ishikawa M, et al. The Benefit of Minced Cartilage Over Isolated Chondrocytes in Atelocollagen Gel on Chondrocyte Proliferation and Migration. *Cartilage* 2021;12(1):93–101. doi: 10.1177/1947603518805205 [published Online First: 2018/10/13] [PubMed: 30311776]

**Key messages:****What is already known about this subject?**

- Several single-cell RNA sequencing studies have been performed on OA knees; however, these studies have been primarily restricted to a single tissue (mainly articular cartilage).
- The majority of cell populations in articular cartilage and meniscus have been identified and characterized.

**What does this study add?**

- Prior scRNA-seq studies included cells from normal tissues, but mainly as comparators to OA tissues. Our study analyzed cells from healthy tissues in detail.
- Our study also provides donor matched articular cartilage and meniscus tissues from both healthy and OA donors.
- Our study identifies a novel pathogenic population that is contributing to disease pathogenesis through a variety of mechanisms including: ECM dysregulation, fibrotic signaling (TGF $\beta$ ), mechanotransduction (tenascin signaling) and cell senescence.
- Our study identifies FAP and ZEB1 as candidate therapeutic targets.

**How might this impact clinical practice or future developments?**

- Our study emphasizes the notion that, understanding OA pathogenesis with the goal of developing novel therapeutic approaches requires careful consideration of whole joint molecular changes.
- FAP and ZEB1 are candidate cross-tissue therapeutic targets.

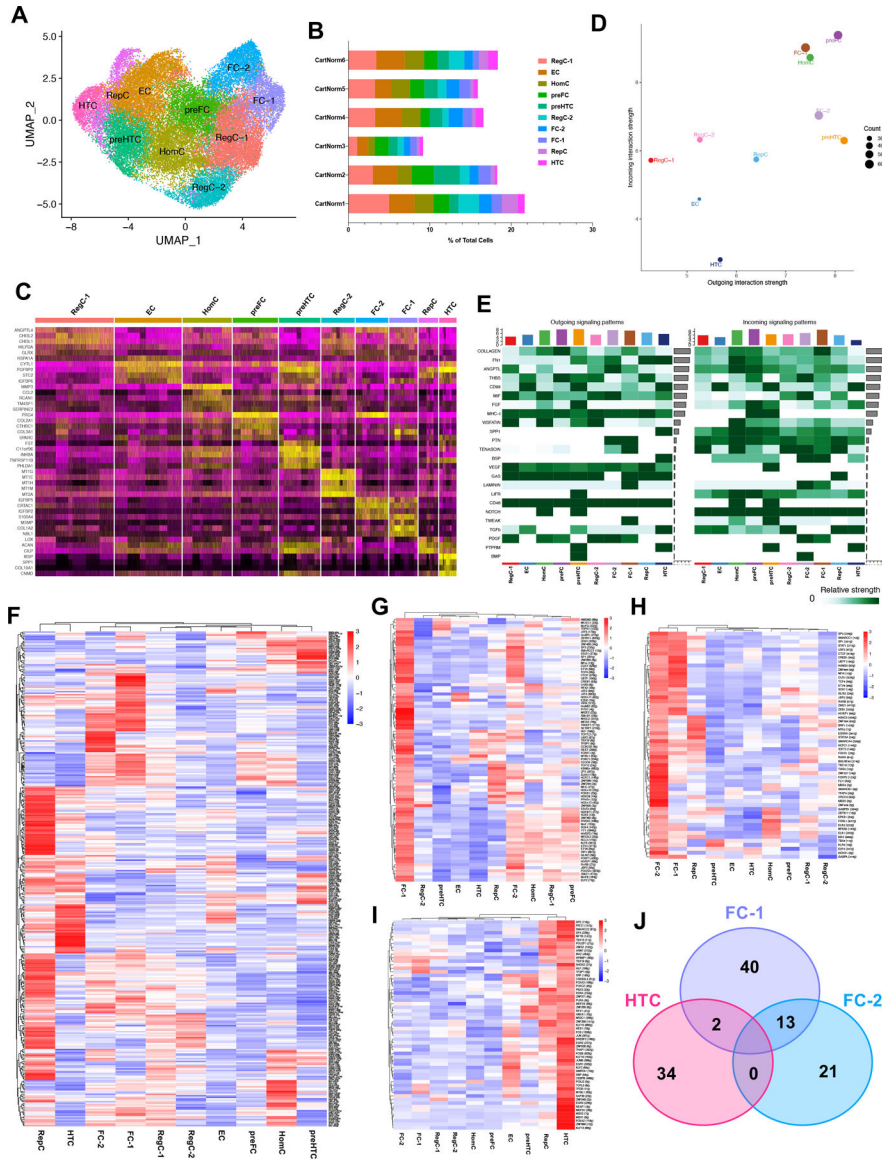


**Figure 1. Single-cell RNA sequencing of healthy human articular cartilage.** (A) Visualization of clustering by UMAP plot of healthy articular cartilage samples. (B) Quantification of individual donor contribution to each cluster shown as percentage of total cell count of the integrated data set. (C) Top 5 markers for each cluster as visualized in a heat-map. (D) CellChat analysis was performed to interrogate cell-cell communication patterns between clusters in articular cartilage. Overall outgoing and incoming signal strength of each cluster was visualized in a scatter plot. (E) Relative strength of all enriched signals (outgoing and incoming) across articular cartilage clusters was visualized in a heat-map. (F) pySCENIC analysis revealed enriched regulons (TF and all promoter-bound gene targets) across all healthy articular cartilage clusters. Relative regulon activity (AUC score) is shown for each regulon for each cluster in a heat-map. (G-H) Heat-maps showing active regulons (AUC > 1) in FC-1 (G), FC-2 (I) and HTC (H). (J) Intersection of active regulons between FC-1, FC-2 and HTC. For all panels: RegC: regulatory chondrocytes,

EC: effector chondrocytes, preFC: pre-fibrocartilage chondrocytes, FC: fibrocartilage chondrocytes, preHTC: pre-hypertrophic chondrocytes, HTC: hypertrophic chondrocytes, HomC: homeostatic chondrocytes and RepC: reparative chondrocytes.

Author Manuscript

Author Manuscript

Author Manuscript

Author Manuscript

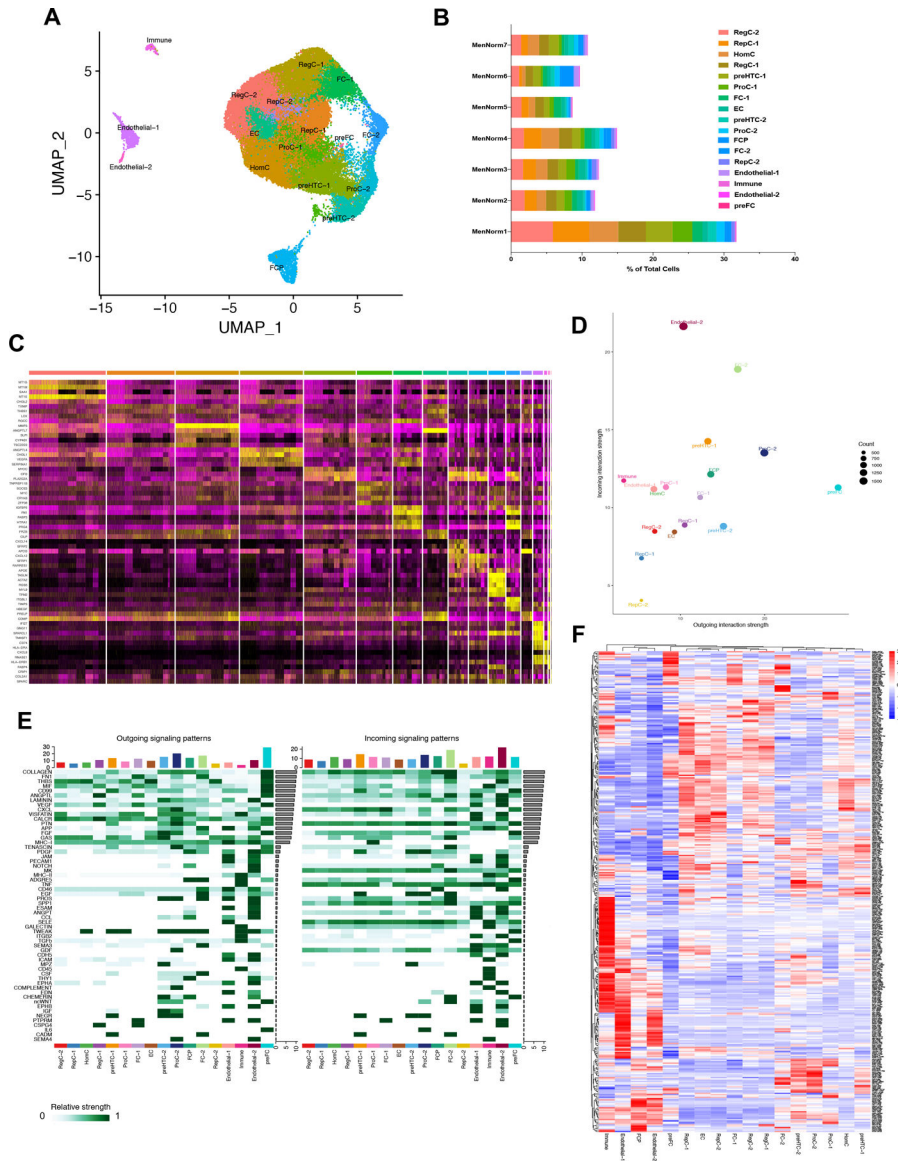


**Figure 2. Single-cell RNA sequencing of healthy human meniscus.** (A) Visualization of clustering by UMAP plot of healthy meniscus samples. (B) Quantification of individual donor contribution to each cluster shown as percentage of total cell count of the integrated data set. (C) Top 5 markers for each cluster as visualized in a heat-map. (D) CellChat analysis was performed to interrogate cell-cell communication patterns between clusters in articular cartilage. Overall outgoing and incoming signal strength of each cluster was visualized in a scatter plot. (E) Relative strength of all enriched signals (outgoing and incoming) across meniscus clusters was visualized in a heat-map. (F) pySCENIC analysis revealed enriched regulons (TF and all promoter-bound gene targets) across all healthy meniscus clusters. Relative regulon activity (AUC score) is shown for each regulon for each cluster in a heat-map. For all panels: RegC: regulatory chondrocytes, EC: effector chondrocytes, preFC: pre-fibrocartilage chondrocytes, FC: fibrocartilage chondrocytes, ProC: proliferative chondrocytes, preHTC: pre-hypertrophic

Author Manuscript

Author Manuscript

Author Manuscript

Author Manuscript

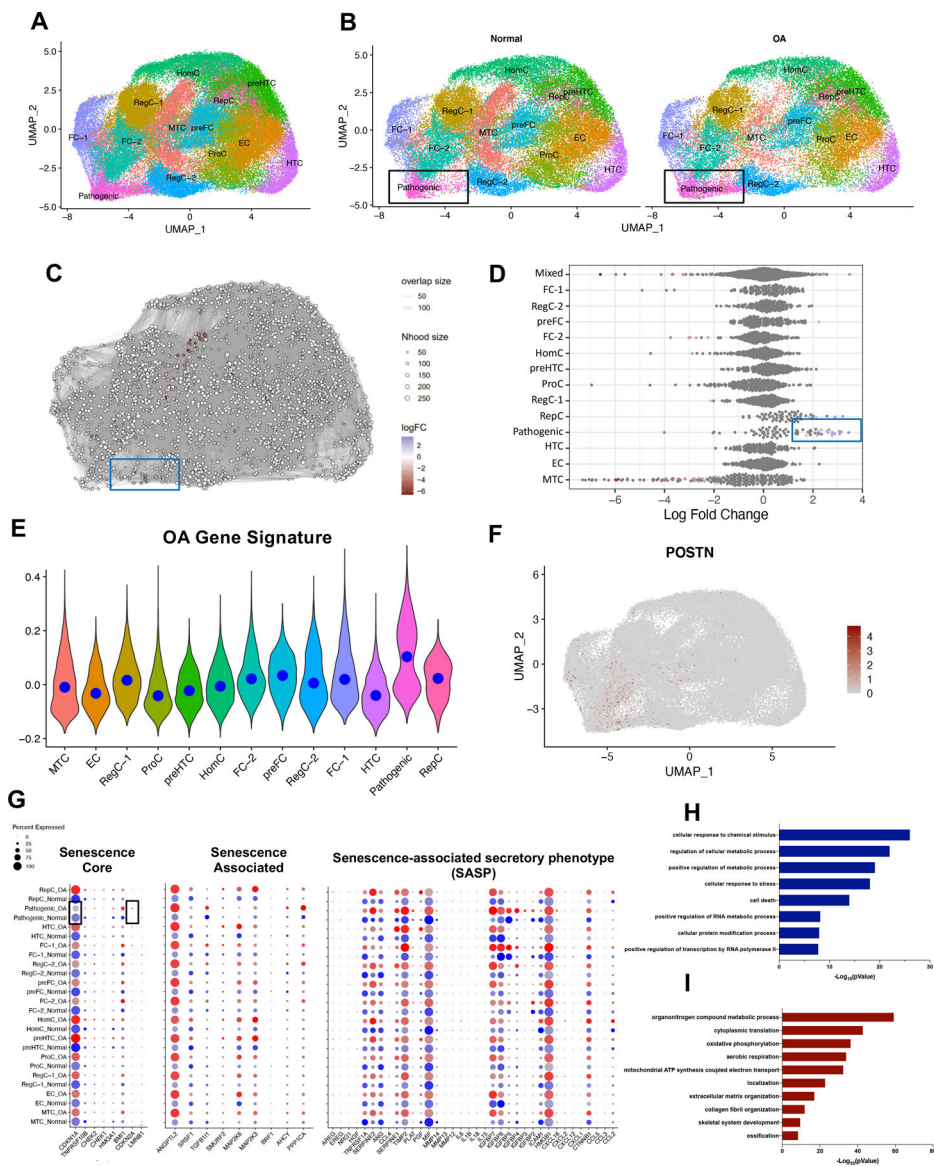
chondrocytes, HomC: homeostatic chondrocytes, RepC: reparative chondrocytes and FCP: fibrocartilage progenitors.

Author Manuscript

Author Manuscript

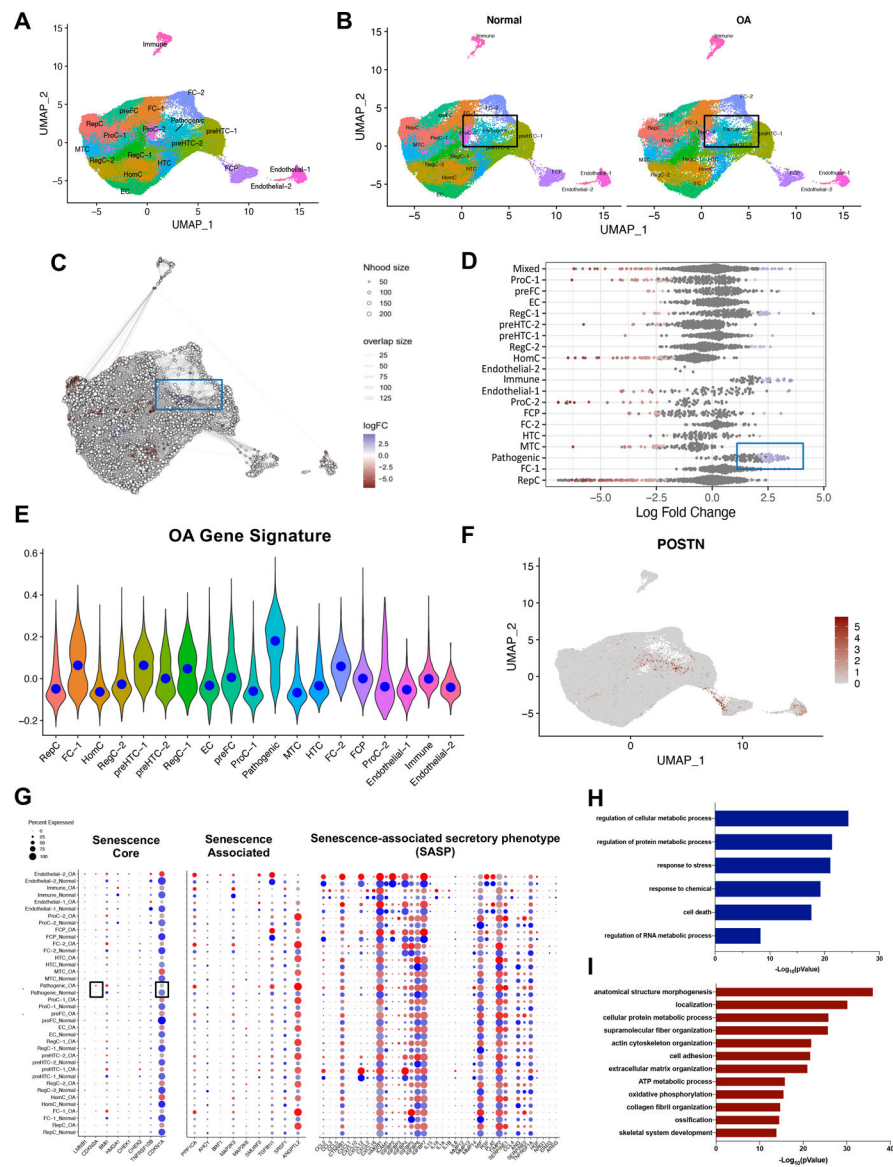
Author Manuscript

Author Manuscript

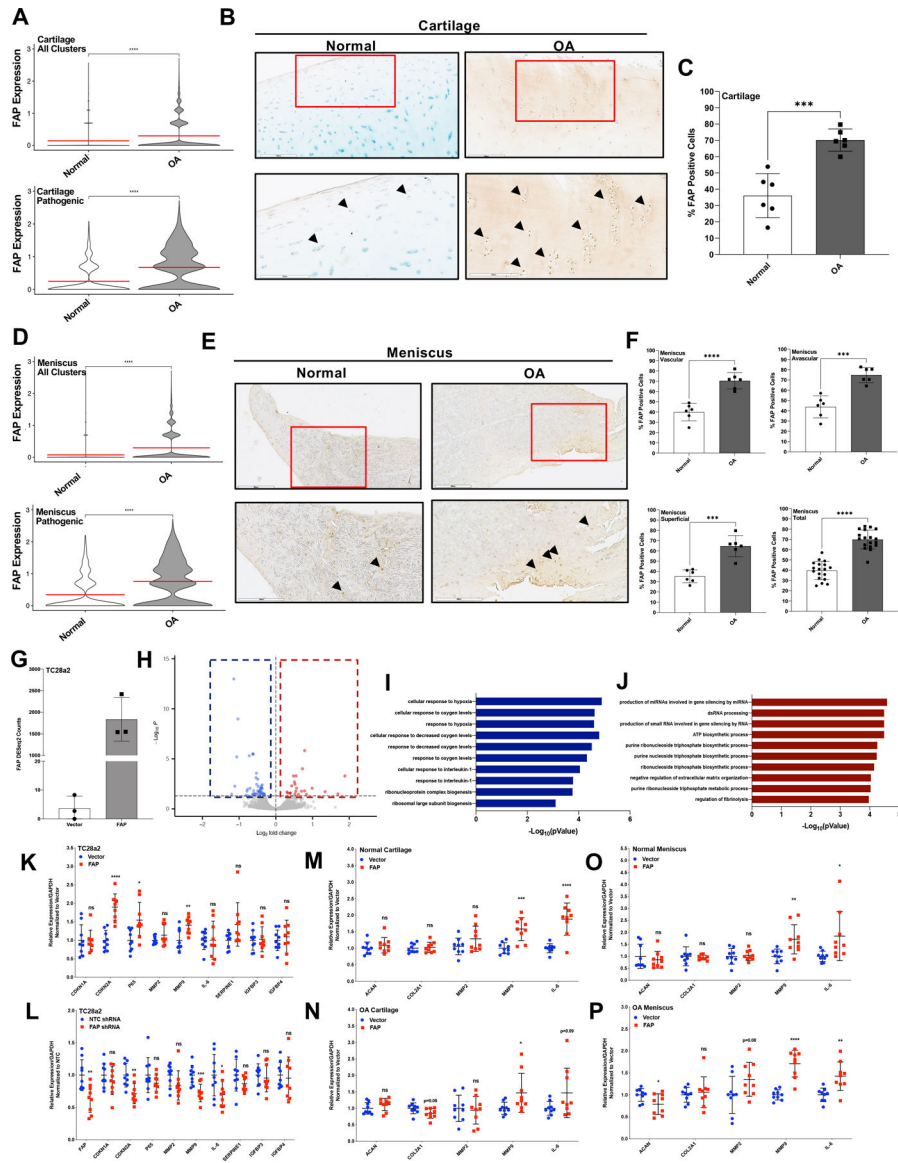


**Figure 3. Identification of a pathogenic population in OA articular cartilage.**

(A) Visualization of clustering by UMAP plot of integrated normal (n=6) and OA (n=6) articular cartilage samples. (B) Identification of a pathogenic population in OA cartilage (black boxes) by visualization of UMAP plot split by condition (normal vs OA). (C, D) Milo analysis revealed differential abundance of cell neighborhoods in OA compared to normal (blue boxes) in the pathogenic subset. (E) An OA gene signature score was assigned to each cell in the integrated dataset and the scores visualized on a violin plot split by cluster. (F) Significant expression of *POSTN* in the pathogenic subset as shown by UMAP plot. (G) Expression of senescence genes (core, associated and SASP) in all clusters split by condition was visualized in bubble plots. Intensity of the color (blue and red) represents relative expression of a gene. Size of the bubble represents the percentage of cells in the cluster expressing the gene. (H, I) GO analysis showing biological processes downregulated (H) and upregulated (I) in the pathogenic subset using gProfiler.

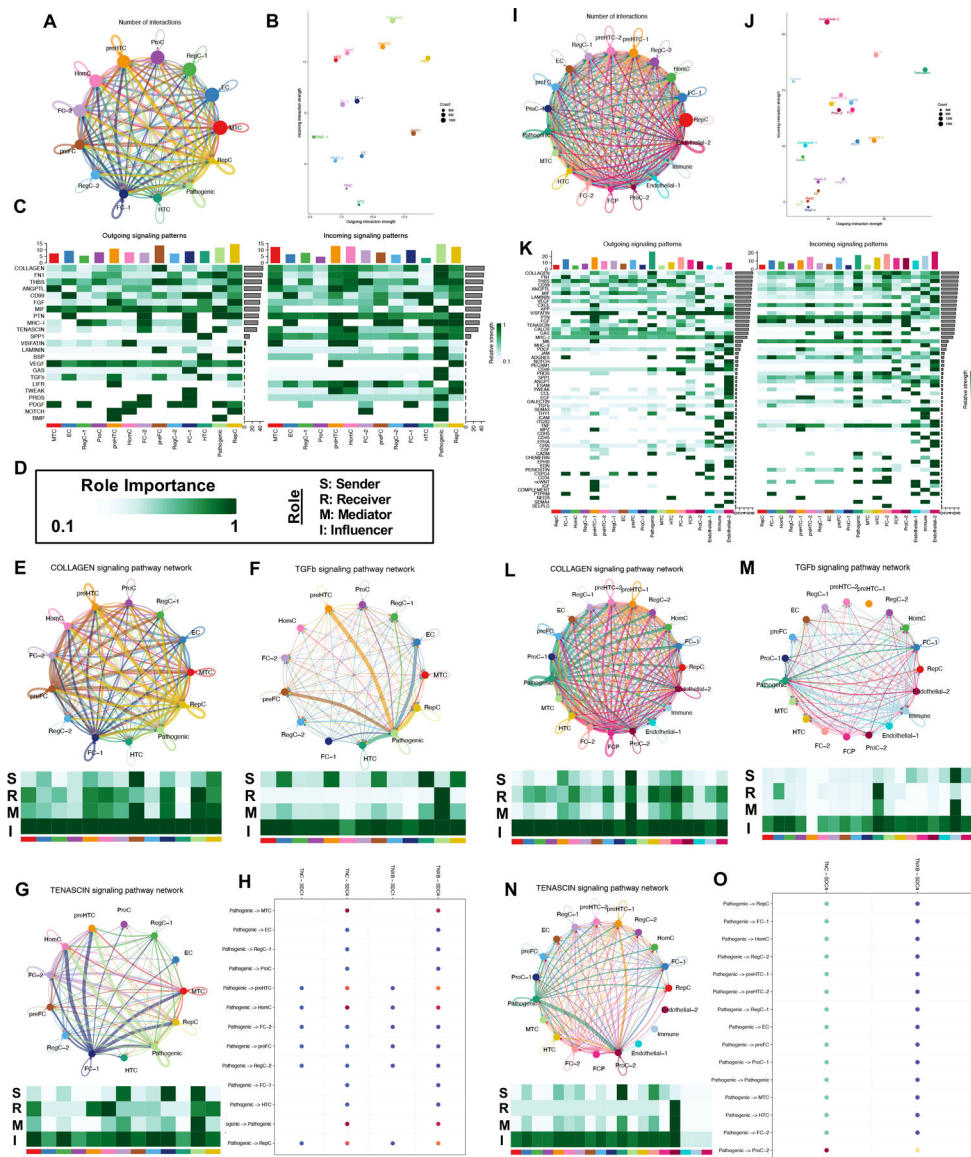


**Figure 4. Identification of a pathogenic population in OA meniscus.** (A) Visualization of clustering by UMAP plot of integrated normal (n=7) and OA (n=6) meniscus samples. (B) Identification of a pathogenic population in OA meniscus (black boxes) by visualization of UMAP plot split by condition (normal vs OA). (C, D) Milo analysis revealed differential abundance of cell neighborhoods in OA compared to normal (blue boxes) in the pathogenic subset. (E) An OA gene signature score was assigned to each cell in the integrated dataset and the scores visualized on a violin plot split by cluster. (F) Significant expression of *POSTN* in the pathogenic subset as shown by UMAP plot. (G) Expression of senescence genes (core, associated and SASP) in all clusters split by condition was visualized in bubble plots. Intensity of the color (blue and red) represents relative expression of a gene. Size of the bubble represents the percentage of cells in the cluster expressing the gene. (H, I) GO analysis showing biological processes downregulated (H) and upregulated (I) in the pathogenic subset using gProfiler.



**Figure 5. FAP promotes OA pathogenesis genes, including *MMP9* and *IL6*.** (A) Violin plots showing upregulation of FAP expression in OA compared to normal across all clusters (**upper**) and specifically in the pathogenic cluster (**lower**) in articular cartilage. (B, C) IHC and quantification of FAP protein in OA compared to normal in articular cartilage. Error bars are standard deviation, n=6. Black arrows indicate positive cells. (D) Violin plots showing upregulation of FAP expression in OA compared to normal across all clusters (**upper**) and specifically in the pathogenic cluster (**lower**) in meniscus. (E, F) IHC and quantification of FAP protein in OA compared to normal in meniscus. Error bars are standard deviation, n=6. Black arrows indicate positive cells. (G) DESeq2 normalized read counts for FAP in FAP-activated TC28a2 cells (n=3) compared to vector control cells (n=3). (H) Volcano plot showing significantly downregulated (blue) and upregulated (red) genes in FAP-activated TC28a2 cells compared to control cells. DEGs were filtered by adjusted p value < 0.05. GO analysis showing biological processes downregulated (I) and

upregulated (**J**) in FAP activation. (**K**) RT-qPCR showing expression of *ACAN*, *COL2A1*, *MMP2*, *MMP9* and *IL6* in FAP-activated TC28a2 cells compared to vector control. (**L**) RT-qPCR as in (**K**) in ZEB1-depleted TC28a2 cells using shRNA. (**M-P**) RT-qPCR as in (**K**) in FAP-activated primary healthy articular cartilage (**M**) healthy meniscus (**O**), OA articular cartilage (**N**) and OA meniscus (**P**) cells. As indicated in each panel, data are relative to GAPDH and normalized to vector control or NTC shRNA. Error bars are standard deviation, n=9 (n=3 biological replicates, n=3 technical replicates/biological replicate). For all panels: \*p<0.05, \*\*p<0.01, \*\*\*p<0.001, \*\*\*\*p<0.0001 by multiple unpaired Student's t tests.



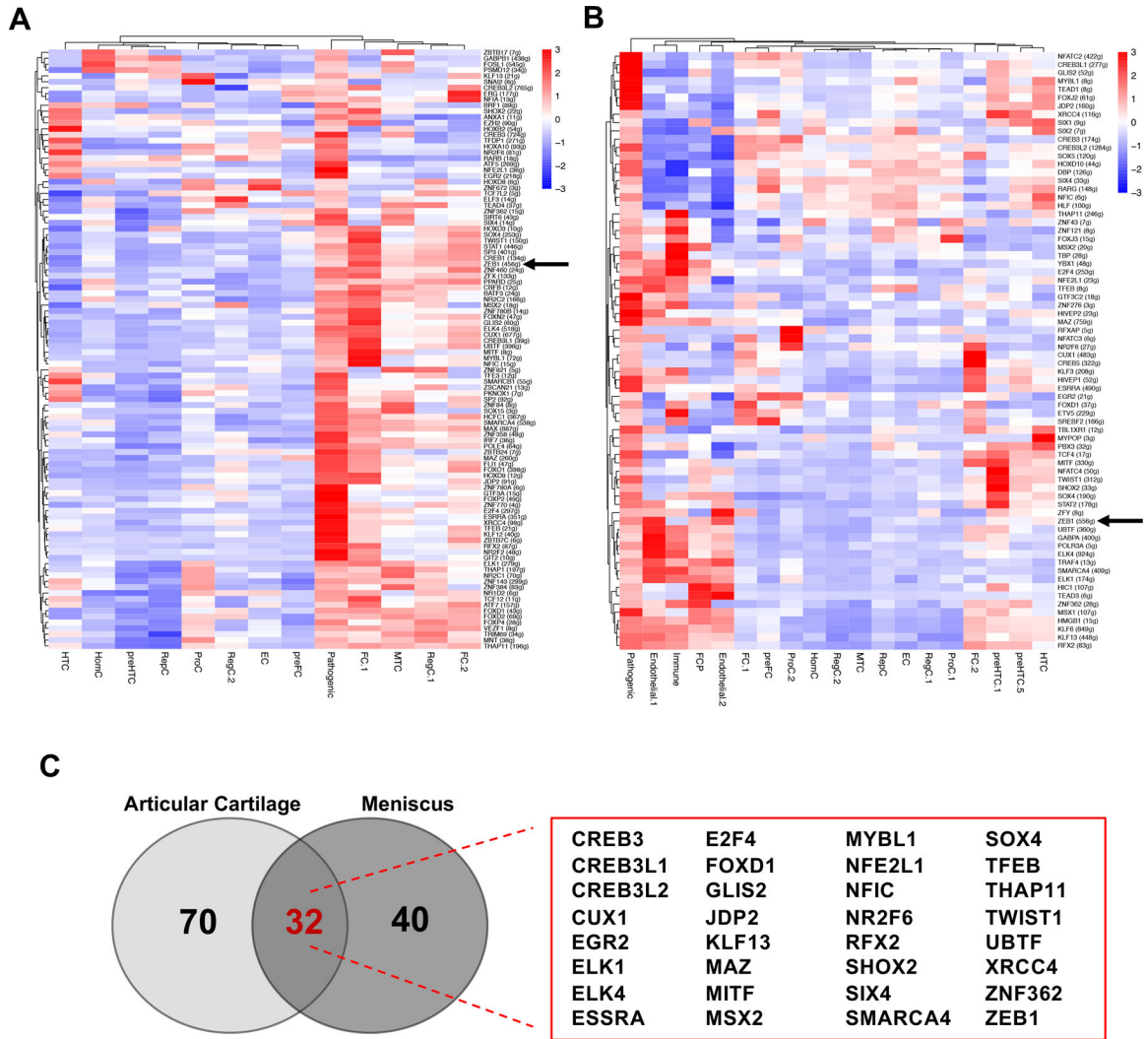


**Figure 7. Identification of shared dysregulated TFs in the pathogenic subset in both tissue types.** (A, B) pySCENIC analysis revealed enriched regulons (> 0.5) in the pathogenic subset in articular cartilage (102 regulons) (A) and meniscus (72 regulons) (B). ZEB1 regulon is marked by black arrows. (C) 32 regulons were shared in this subset between both tissue types.

Author Manuscript

Author Manuscript

Author Manuscript

Author Manuscript

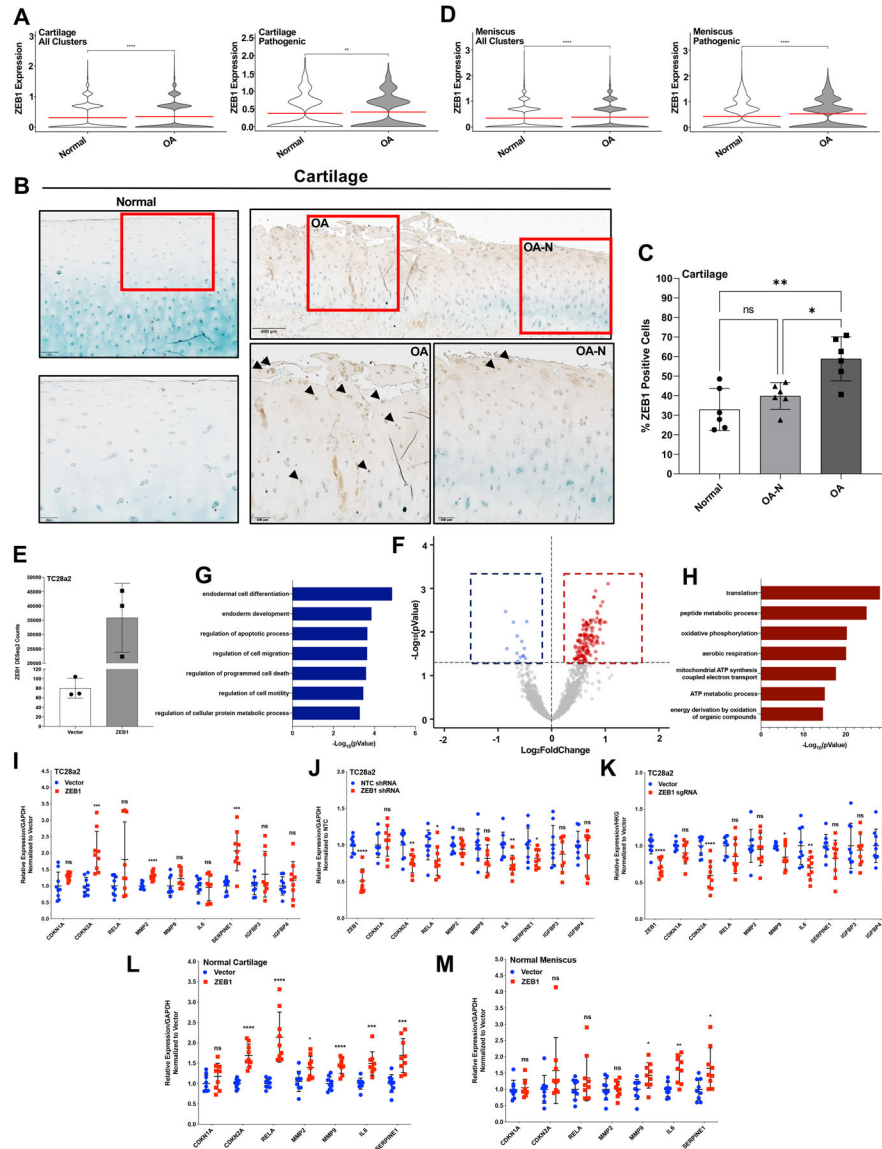


**Figure 8. ZEB1 promotes mitochondrial dysregulation and p16-induced cell senescence.** (A) Violin plots showing upregulation of ZEB1 expression in OA compared to normal across all clusters (left) and specifically in the pathogenic cluster (right) in articular cartilage. (B, C) IHC and quantification of ZEB1 protein in OA compared to normal in articular cartilage. ZEB1 protein in OA-affected area (OA) and normal-appearing area (OA-N) from the same OA donor are shown. Error bars are standard deviation, n=6. \*p<0.05, \*\*p<0.01 by One-Way ANOVA test with multiple comparisons. (D) Violin plots showing upregulation of ZEB1 expression in OA compared to normal across all clusters (left) and specifically in the pathogenic cluster (right) in meniscus. (E) DESeq2 normalized read counts for ZEB1 in ZEB1-activated TC28a2 cells (n=3) compared to vector control cells (n=3). (F) Volcano plot showing significantly downregulated (blue) and upregulated (red) genes in ZEB1 activated TC28a2 cells compared to control cells. DEGs were filtered by adjusted p value < 0.05. GO analysis showing biological processes downregulated (G)

and upregulated (**H**) in ZEB1 activation using gProfiler. (**I**) RT-qPCR showing expression of *CDKN1A*, *CDKN2A*, *RELA*, *MMP2*, *MMP9*, *IL6* and *SERPINE1* in ZEB1-activated TC28a2 cells compared to vector control. (**J**, **K**) RT-qPCR as in (**I**) in ZEB1-depleted TC28a2 cells using shRNA (**J**) and CRISPRi (**K**). (**L**, **M**) RT-qPCR as in (**I**) in ZEB1-activated primary articular cartilage (**L**) and primary meniscus (**M**) cells. As indicated in each panel, data are relative to either GAPDH, or the geometric mean of three housekeeping genes (HKG; GAPDH, PGK1 and  $\beta$ 2M) and normalized to vector control or NTC shRNA. Error bars are standard deviation, n=9 (n=3 biological replicates, n=3 technical replicates/biological replicate). For all panels: \*p<0.05, \*\*p<0.01, \*\*\*p<0.001, \*\*\*\*p<0.0001 by multiple unpaired Student's t tests.